PERGAMON

Deep-Sea Research I 49 (2002) 101–120

DEEP-SEA RESEARCH
PART I

www.elsevier.com/locate/dsr

A two-tracer (^{210}Po–^{234}Th) approach to distinguish organic carbon and biogenic silica export flux in the Antarctic Circumpolar Current

Jana Friedrich*, Michiel M. Rutgers van der Loeff

Alfred Wegener Institute for Polar and Marine Research, P.O. Box 120161, D-27515 Bremerhaven, Germany

Received 21 March 2000; received in revised form 14 March 2001; accepted 9 July 2001

Abstract

We attempt to quantify and qualify the particle export from the surface water of the Antarctic Circumpolar Current during a spring phytoplankton bloom by the simultaneous use of the tracers ^{210}Po and ^{234}Th. We present data from the Southern Ocean JGOFS expedition in 1992 at about 6°W, from the marginal ice zone to the Polar Frontal region. Radionuclide export was calculated with a one-dimensional non-steady-state scavenging model. Rapidly changing activities of ^{210}Pb and ^{210}Po during the phytoplankton bloom and the application of the tracer pair ^{210}Po/^{210}Pb with particle-reactive parent and daughter required a new solution to the non-steady-state scavenging model. The observed fractionation of ^{210}Po and ^{234}Th on particles, dependent on particle composition (POC/biogenic silica ratio), corroborates the known preference of ^{210}Po for cytoplasm. A combination of these two tracers can help to characterize the nature (i.e. organic carbon and biogenic silica content) of the material settling out of the mixed layer, and thus to arrive at a more detailed interpretation of export fluxes than is possible with ^{234}Th alone. In the Polar Front region, where diatoms are dominant in the phytoplankton and where the highest export rates were observed, we find a preferential settling of biogenic silica when heavily silicified diatom species occur. In contrast, POC and biogenic silica are exported with comparable efficiency when diatom species with thinner frustules prevail. The export of biogenic opal and carbon is then closely coupled. In the southern Antarctic Circumpolar Current (sACC), where siliceous organisms are not dominant in the plankton, we find a preferential settling of siliceous material over POC.

Keywords: Radionuclides; Tracers; Organic carbon; Biogenic silica; Export; Antarctic Circumpolar Current

1. Introduction

The export of particles from the euphotic zone to the deep plays a crucial role in the marine carbon cycle. Direct measurements of particle fluxes with sediment traps (Fischer et al., 1988; Wefer and Fischer, 1991) and indirect estimates from particle reactive radionuclide export rates are well known. Since these radionuclides are produced and decay at known rates, they provide a good tool to quantify particle export (Cherry et al., 1975; Kharkar et al., 1976; Bacon and Anderson, 1982; Fisher et al., 1988). With knowledge of the

*Corresponding author. GeoForschungsZentrum Potsdam, Telegrafenberg, PB 5.1, D-14473 Potsdam, Germany. Tel.: +49-331-288-1506; fax: +49-331-288-1570.

E-mail address: janaf@gfz-potsdam.de (J. Friedrich).

0967-0637/01/$ - see front matter
PII: S0967-0637(01)00045-0

Nomenclature

AASW	Antarctic Surface Water
ACC	Antarctic Circumpolar Current
AWB	Antarctic Weddell Gyre Boundary
BSi	biogenic silica
MIZ	marginal ice zone
PFr	Polar Frontal region
POC	particulate organic carbon
PPC	phytoplankton carbon
sACC	southern Antarctic Circumpolar Current
SACCF	southern Antarctic Circumpolar Current Front
UCDW	Upper Circumpolar Deep Water
WF	Weddell Front

fluxes and the adsorption behavior of the radionuclides, it is possible to make good estimates of carbon export (Moore and Dymond, 1988; Buesseler et al., 1992). For this approach ^{234}Th is very often the radionuclide of choice. It is produced through the decay of its parent nuclide ^{238}U at known rates and is highly particle reactive, and its half life of 24.1 days is very suitable especially for tracing events on a short time scale like the development of a phytoplankton bloom and subsequent particle export (Buesseler et al., 1995; Rutgers van der Loeff et al., 1997). Murray et al. (1989), and Shimmield et al. (1995) pointed out that ^{234}Th possibly tracks the total mass flux rather more closely than the POC flux. There is a need to introduce a tracer that can help to characterize the nature of the material settling out of the euphotic zone. Thus, one can arrive at a more detailed interpretation of export fluxes than is possible with ^{234}Th alone. The use of ^{210}Po and ^{210}Pb as tracers for particle transport was shown by Rama et al. (1961), Craig et al. (1973), Turekian et al. (1974) and others. ^{210}Po and ^{210}Pb export from the euphotic zone and regeneration rates within the thermocline have usually been calculated with traditional steady-state models (Bacon et al., 1976; Nozaki and Tsunogai, 1976; Ritchie and Shimmield, 1991; Shimmield et al., 1995; Sarin et al., 1999). Buesseler et al. (1992), and Rutgers van der Loeff et al. (1997) showed that steady-state transport models have disadvantages in the case of very rapidly varying fluxes caused by phytoplankton bloom events.

^{210}Pb and ^{210}Po are produced at the end of the ^{238}U decay chain. ^{210}Pb ($t^{1/2} = 22.3$ a) is delivered in situ by decay of its longer-living grandparent ^{226}Ra, and from the atmosphere by precipitation. ^{210}Po is almost exclusively supplied in situ by decay of its grandparent ^{210}Pb. The ^{210}Po/^{210}Pb disequilibrium integrates export on a longer timescale than ^{234}Th/^{238}U and complements the ^{234}Th/^{238}U disequilibrium, which integrates particle export on a timescale of several weeks.

The aim of the 1992 SO-JGOFS expedition of R.V. *Polarstern* was to investigate the development of a spring phytoplankton bloom in the Atlantic sector of the Antarctic Southern Ocean including the Polar Frontal region (PFr), the southern Antarctic Circumpolar Current zone (sACC), its boundary with the Weddell Gyre (AWB) and the marginal ice zone (MIZ). The development of distinct phytoplankton blooms in the PFr, dominated by different diatom species, contrasted with the poverty of the MIZ and the frontal region of the AWB (Smetacek et al., 1997). The blooms in the PFr were detected by the distribution of chlorophyll *a* (Bathmann et al., 1997) and primary productivity (Jochem et al., 1995). In the southern ACC, chlorophyll stocks remained low throughout the study (Bathmann et al., 1997). An extended description of the ecologic situation in the investigation area is given in Smetacek et al. (1997).

In a previous paper, (Rutgers van der Loeff et al., 1997) we presented the ^{234}Th export rate as tracer for particle export from the surface water. In this approach, the uncertainty in estimating corresponding carbon export rates lies primarily in the POC/^{234}Th ratio of the particles actually settling. Here, we present for the same expedition the export flux of ^{210}Pb and ^{210}Po out of the euphotic zone during the phytoplankton bloom, calculated with the non-steady-state solution of a one-dimensional scavenging model. Using the joint dataset, we developed a two-tracer model (^{210}Po–^{210}Pb and ^{210}Po–^{234}Th) to characterize the nature (i.e. organic carbon and biogenic silica

content) of the material settling out of the mixed layer.

2. Material and methods

The study area of the SO JGOFS expedition with R.V. *Polarstern* during October–December 1992 including the stations of radionuclide sampling is shown in Fig. 1. Samples were taken along three longitudinal transects (6°W) at the beginning (2 Oct–18 Oct = transect 2), middle (22 Oct–30 Oct = transect 5) and end of spring 10 Nov–21 Nov = transect 11). Seawater samples were collected with 270-l Gerard bottles usually at 20, 60, 100, 200, 400 and 600 m depths. Immediately after recovering the bottles, the water was pumped with a centrifugal pump through a 142 mm diameter, 1 μm Nuclepore filter. The filtered volume was measured with a KENT flow meter. Immediately after the filtration, a 20 kg aliquot of filtrate was weighed, acidified with 20 ml of HNO_3, and spiked with ^{230}Th, ^{208}Po and stable Pb yield tracers. 250 mg of Fe was added, and after one-day isotope equilibration NH_3 was added to increase the pH to 8.5, thus co-precipitating Th, Po and Pb with

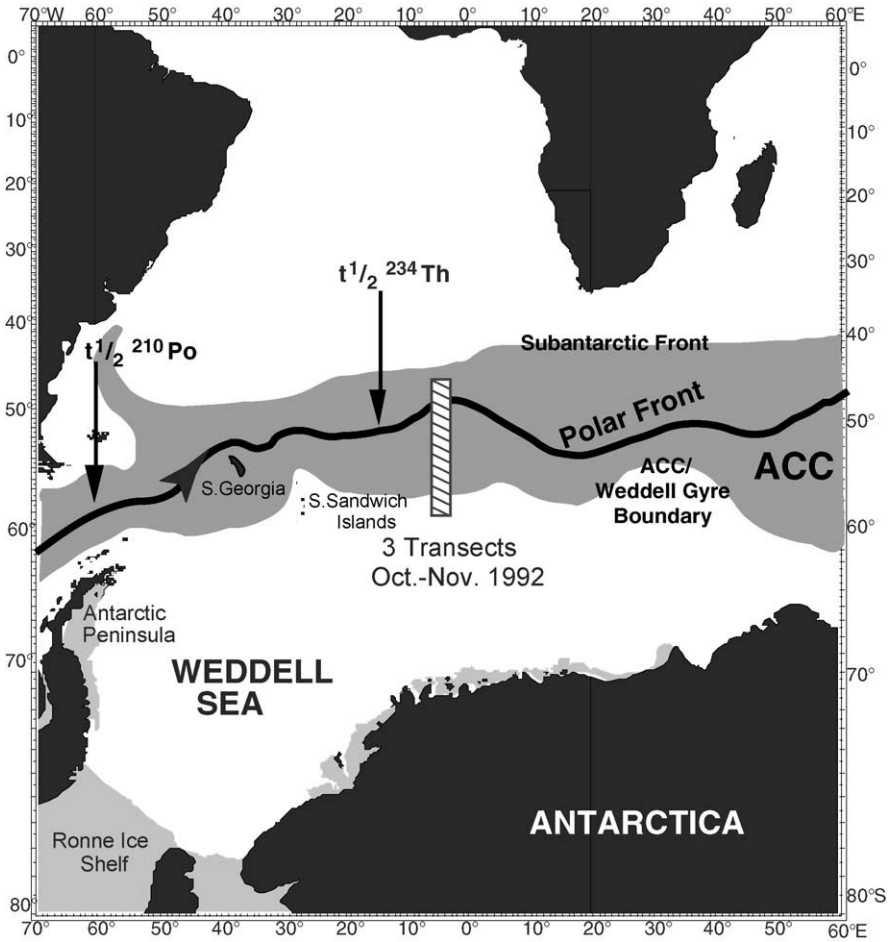

Fig. 1. Map of study area with transects (hatched strip). Average position of the major fronts after Peterson and Stramma (1991). The half-life arrows indicate the distance the surface water of the Antarctic Circumpolar Current travels eastward (30 cm s^{-1}, Whitworth and Nowlin, 1987) to the study area during the decay time of ^{234}Th (24 days) and ^{210}Po (138 days).

$Fe(OH)_3$. The hydroxide precipitate was collected by settling and centrifugation, and dissolved in a minimum amount of 9 N HCl. After diluting to 0.5 N HCl Fe was complexed with ascorbic acid and Po was plated on silver planchets according to Fleer and Bacon (1984) based on the procedure of Flynn (1968). After Po precipitation, Th was purified according to Anderson and Fleer (1982), leaving the Pb fraction in the eluate of the 8 N HNO_3 column. The entire procedure was carried out on board ship, lasting 2–3 days from sampling to electroplating of Th.

The filter samples were decomposed by microwave acid digestion in a mixture of 10 ml HNO_3, 0.5 ml HF and 2 ml H_2O_2 in the home lab. Organic residues were destroyed by addition of 2 ml $HClO_4$ after spiking with ^{230}Th, ^{208}Po and stable Pb yield tracers. Radionuclide analysis of the filter samples was performed by the same procedures as used for the water samples.

^{210}Pb activity of water and filter samples was determined through the ingrowth of ^{210}Po. The eluate of the 8 N HNO_3 column, containing the Pb fraction, was stored for about one year to allow new ^{210}Po to grow into equilibrium with the ^{210}Pb. Then Po was extracted by the method mentioned above (Flynn, 1968). The chemical yield of the added stable Pb was determined by atomic adsorption spectrometry.

The silver planchets with the Po fraction were measured by alpha counting on silicon surface-barrier detectors (EG&G Ortec) until a minimum of 500 counts was reached. ^{210}Pb and ^{210}Po activities are calculated and decay- and ingrowths-corrected to the time of sampling according to Fleer and Bacon (1984). Error estimates (1-sigma) include counting errors and uncertainties in blanks, spike activities and sample volume. An extended description of the analytical procedure and error discussion is given in Friedrich (1997).

The ^{226}Ra activity was calculated from the silica concentration of the water from the relationship of Ku and Lin (1976)

$$^{226}\mathrm{Ra}\,(\mathrm{dpm}\,100\,\mathrm{kg}^{-1}) = 13 + 0,072 \times \mathrm{Si}(\mu\mathrm{M}).$$

This relationship applies to waters south of the Polar Front. Suspended particulate matter (SPM) concentrations were calculated from transmissometer data. The transmission values at the depth of the radionuclide sampling were interpolated from the continuous hydrocast profiles and converted into suspended load applying the algorithm by Gardner et al. (1993), described in Rutgers van der Loeff et al. (1997). Samples for particulate organic carbon (POC) measurements were taken from the same depth as the radionuclide samples. The analysis procedure is described in Bathmann et al. (1997). POC values were taken from Bathmann et al. (1997), and biogenic silica was measured by Quéguiner et al. (1997). These data are available on CD-ROM (Rommets et al., 1997).

3. Results

First, we describe the radionuclide distribution in the study area in general, and then we pay attention to the changes during to the developing phytoplankton bloom. The radionuclide, POC and biogenic silica data from 20 to 200 m depth are listed in Table 1. The complete dataset is available at www.pangaea.de/ftp and on CD-ROM (Rommets et al., 1997). The total ^{210}Pb and ^{210}Po distribution in the upper 600 m of the water column is shown for transect 11 in Fig. 2a and b, as an example.

The depth of the mixed layer ranged from 100 m in the Antarctic Zone (56–57°S) to 80 m in the PFr (Veth et al., 1997). The depth of the euphotic zone ranged from 126 m in the Antarctic Zone to 57 m in the PFr (Quéguiner et al., 1997).

The comparison of temperature, salinity and density features (Veth et al., 1997) with those of ^{226}Ra, ^{210}Pb and ^{210}Po (^{226}Ra calculated from silica, Table 1, Fig. 2a and b), shows that the distribution of these radionuclides is primarily determined by water masses within the ACC. The distribution of ^{210}Pb and of ^{210}Po is determined by the ^{226}Ra distribution in the ocean. In the Antarctic Surface Water (AASW) we measured 8–11 dpm ^{210}Pb 100 l^{-1} and 5–7 dpm ^{210}Po 100 l^{-1}. ^{210}Pb activity increased with depth and, in the surface water, from north to south. The ^{210}Pb distribution is in agreement with the one found by

Table 1
Radionuclide, POC and biogenic silica data from 20 to 200 m depth used for the export calculations. POC (Bathmann et al., 1997) and biogenic silica (Quéguiner et al., 1997) in mmol 100 L^{-1}, ^{226}Ra activity calculated from silica after Ku and Lin (1976), ^{210}Pb and ^{210}Po data (dpm 100l^{-1}) with propagated 1-sigma errors, and ^{234}Th (from Rutgers van der Loeff et al., 1997)

Stat.	Depth (m)	Lat (°S)	POC (mmol 100l^{-1})	Silica (mmol 100l^{-1})	^{226}Ra (dpm 100l^{-1})	$^{210}Pb_{dissolved}$ (dpm 100l^{-1})	$^{210}Pb_{particulate}$ (dpm 100l^{-1})	$^{210}Po_{dissolved}$ (dpm 100l^{-1})	$^{210}Po_{particulate}$ (dpm 100l^{-1})	$^{234}Th_{dissolved}$ (dpm 100l^{-1})	$^{234}Th_{particulate}$ (dpm 100l^{-1})
868	20	57°		0.03	18.06	10.19±0.38	0.41±0.04	7.03±0.26	1.06±0.05	235.4±8.2	16.5±1.7
868	60	57°		0.03	18.09	10.37±0.34	0.52±0.06	6.03± 0.18	1.85±0.09	218.3±7.6	30.3±1.8
868	100	57°		0.02	18.48	12.88±0.56	0.45±0.03	5.28±0.23	0.57±0.04	215.7±7.6	5.2±0.3
868	200	57°		0.02	19.65	13.03±0.48	0.59±0.07	7.11±0.25	0.72±0.05	255.7±9.0	11.0±1.2
872	20	55°		0.04	16.32	9.34±0.30	0.50±0.04	8.18±0.25	1.32±0.06	234.6±8.2	9.7±0.4
872	60	55°		0.04	16.28	8.64±0.30	1.10±0.07	6.80±0.22	1.84±0.10	211.6±7.4	37.0±0.9
872	100	55°		0.04	16.35	10.86±0.40	0.57±0.05	4.73±0.17	1.28±0.08	213.5±7.5	11.4±0.4
872	200	55°		0.03	17.31	10.78± 0.43	1.61±0.06	4.70±0.18	1.46±0.07	222.0±7.8	25.6±0.6
876	20	53°		0.03	16.33	9.23±0.36	0.39±0.04	5.88±0.22	1.18±0.06	204.8±7.2	10.8±0.4
876	60	53°		0.03	16.46	9.21±0.29	0.62±0.07	5.79±0.18	1.20±0.06	211.4±7.4	16.9±7.2
876	100	53°		0.03	16.48	10.09±0.36	1.45±0.07	4.87±0.17	0.96±0.04	241.9±8.5	8.0±0.3
876	200	53°		0.02	18.40	12.96±0.60	0.91±0.08	6.32±0.28	0.97±0.04	245.2±8.6	12.7±0.4
877	20	49°		0.19	14.88	8.35±0.44	0.34±0.02	6.45±0.34	1.66±0.08	197.4±6.9	31.1±0.9
877	60	49°		0.22	14.88	10.33±0.72	0.36±0.02	4.56±0.31	0.90±0.04	189.0±6.6	25.7±0.7
877	100	49°		0.18	14.94	8.80±0.40	0.70±0.05	7.74±0.34	1.48±0.06	220.1±7.7	51.2±0.9
877	200	49°		0.06	15.60	9.00±0.45	1.16±0.05	4.80±0.24	1.04±0.05	249.1±8.7	24.6±0.6
879	20	48°	0.93	0.20	14.78	9.23±0.52	0.32±0.04	5.94±0.33	1.54±0.08	181.8±6.4	33.6±0.8
879	60	48°	0.76	0.16	14.81	8.09±0.42	0.51±0.05	4.54±0.23	1.13±0.06	192.9±6.8	39.7±0.9
879	200	48°	0.21	0.05	15.64	10.53±0.76	0.61±0.10	4.70±0.33	0.44±0.03	212.7±7.4	10.6±0.3
886	20	56°			17.09	8.95±0.50	0.28±0.02	7.15±0.40	1.43±0.08	216.1±7.6	8.5±0.4
886	45	56°			17.07	9.25±0.63	0.43±0.03	6.55±0.44	1.75±0.11	216.0±7.6	23.0±1.0
886	100	56°			17.03	8.14±0.47	0.28±0.02	5.03±0.29	1.01±0.07	211.4±7.4	8.4±0.5
886	200	56°			18.52	11.15±0.66	0.40±0.02	5.96±0.35	0.73±0.05	246.3±8.6	7.4±0.3
891	20	55°		0.02	16.24	8.03±0.39	0.13±0.02	6.34±0.30	1.23±0.07	225.9±7.9	12.7±0.4
891	60	55°		0.03	16.25	9.60±0.46	0.42±0.04	3.19±0.15	1.08±0.08	234.4±8.2	9.0±0.6
891	100	55°		0.03	16.27	8.72±0.43	0.35±0.03	5.19±0.25	1.11±0.08	232.8±8.1	9.9±0.4
891	200	55°		0.02	17.55	10.77±0.51	0.23±0.02	5.33±0.25	0.48±0.05	233.8±8.2	4.9±0.2
895	20	53°		0.02	15.97	8.28±0.36	0.30±0.03	5.64±0.24	1.20±0.11	219.1±7.7	9.5±0.6
895	60	53°		0.02	15.97	9.15±0.44	0.43±0.03	5.79±0.27	1.38±0.08	220.0±7.7	20.5±0.7
895	100	53°		0.03	16.00	8.67±0.40	0.21±0.02	5.64±0.25	0.73±0.06	197.7±6.9	10.3±0.5
895	200	53°		0.02	17.28	10.96±0.48	0.42±0.03	4.62±0.20	0.70±0.06	242.9±8.5	10.2±0.4
899	20	51°	0.49	0.04	15.42	8.11±0.40	0.18±0.03	5.52±0.27	1.31±0.11	201.9±7.1	13.6±0.5
899	60	51°	0.67	0.04	15.46	8.36±0.41	0.43±0.04	4.17±0.20	1.14±0.11	212.0±7.4	23.0±0.7
899	100	51°	0.66	0.06	15.51	8.94±0.45	0.38±0.06	3.90±0.19	0.60±0.07	196.1±6.9	14.7±0.6
899	200	51°	0.47	0.06	16.96	10.97±0.60	0.38±0.03	5.35±0.29	0.86±0.07	233.7±8.2	12.1±0.4
903	20	49°	1.42	0.44	14.22	6.93±0.25	1.01±0.10	5.38±0.19	1.99±0.10	161.2±5.6	53.7±1.6

(*continued on next page*)

Table 1 (*continued*)

Stat.	Depth (m)	Lat (°S)	POC (mmol 1001^{-1})	Silica (mmol 1001^{-1})	^{226}Ra (dpm 1001^{-1})	$^{210}Pb_{dissolved}$ (dpm 1001^{-1})	$^{210}Pb_{particulate}$ (dpm 1001^{-1})	$^{210}Po_{dissolved}$ (dpm 1001^{-1})	$^{210}Po_{particulate}$ (dpm 1001^{-1})	$^{234}Th_{dissolved}$ (dpm 1001^{-1})	$^{234}Th_{particulate}$ (dpm 1001^{-1})
903	60	49°	1.48	0.63	14.32	7.92±0.38	1.27±0.11	4.24±0.20	1.61±0.08	161.0±5.6	56.8±1.4
903	100	49°	0.73	0.46	14.91	7.58±0.41	0.68±0.05	3.67±0.20	1.10±0.07	182.7±6.4	41.3±1.0
903	200	49°	0.24	0.12	16.01	9.13±0.45	0.55±0.04	5.02±0.24	0.86±0.05		13.7±0.5
907	20	47°	1.24	0.27	14.34	8.54±0.41	0.47±0.04	5.07±0.24	1.67±0.13	168.2±5.9	56.5±1.6
907	43	47°	1.15	0.30	14.34	8.65±0.34	0.64±0.05	4.85±0.18	2.05±0.14	182.2±6.4	69.4±1.8
907	100	47°	0.82	0.70	14.66	8.70±0.38	0.47±0.07	3.51±0.15	0.85±0.08	177.9±6.2	36.2±1.3
907	200	47°	0.38	0.124	15.39	9.87±0.37	0.50±0.03	4.25±0.15	0.66±0.05	222.1±7.8	15.6±0.5
941	20	57°	0.66	0.055	17.78	10.81±0.49	0.35±0.03	4.47±0.20	1.36±0.06	215.8±7.6	7.7±0.4
941	60	57°	0.64	0.066	17.79	9.75±0.38	0.59±0.04	6.17±0.23	1.61±0.06	223.6±7.8	16.6±0.5
941	100	57°	0.35	0.041	17.99	10.53±0.40	0.29±0.03	5.35±0.20	0.97±0.045	217.7±7.6	9.2±0.4
941	200	57°	0.22	0.02	19.38	12.95±0.50	0.57±0.03	7.48±0.28	0.92±0.04	234.7±8.2	6.4±0.3
945	20	55°		0.041	16.53	8.70±0.40	0.37±0.02	4.55±0.20	1.00±0.04	199.6±7.0	9.5±0.5
945	60	55°		0.042	16.51	9.73±0.46	0.37±0.02	5.77±0.26	1.31±0.05	212.8±7.4	15.3±0.6
945	100	55°		0.065	16.53	10.91±0.64	0.17±0.02	3.84±0.22	0.85±0.04	215.6±7.5	11.8±0.5
945	200	55°		0.025	17.59	11.24±0.53	0.68±0.03	5.16±0.24	0.75±0.03	221.7±7.8	8.6±0.4
949	20	53°	0.44	0.014	16.12	9.09±0.34	0.13±0.02	4.88±0.20	0.97±0.04	205.6±7.2	7.7±0.3
949	60	53°	0.39	0.012	16.14	10.06±0.42	0.17±0.02	5.47±0.22	0.97±0.04	213.4±7.5	13.8±0.5
949	100	53°	0.36	0.016	16.22	8.51±0.45	0.10±0.02	4.66±0.24	0.93±0.04	182.8±6.4	8.9±0.4
949	200	53°	0.32	0.018	17.40	11.13±0.62	0.34±0.03	4.35±0.24	0.60±0.03	226.1±7.9	8.3±0.3
953	20	51°	0.92	0.042	15.29	9.17±0.34	0.07±0.02	5.72±0.20	0.79±0.04	187.9±6.6	13.4±0.7
953	60	51°	0.88	0.029	15.31	7.93±0.43	0.14±0.02	4.96±0.27	1.00±0.04	182.2±6.4	21.3±0.8
953	100	51°	0.53	0.03	15.41	8.29±0.44	0.14±0.02	3.53±0.18	0.44±0.03	190.7±6.7	14.3±0.5
953	200	51°	0.34	0.048	16.47	10.42±0.50	0.23±0.02	3.72±0.18	0.44±0.03	218.4±7.6	9.6±0.3
960	20	49°	1.95	0.597	13.81	6.66±0.38	1.15±0.08	5.92±0.34	1.83±0.07	138.2±4.8	46.5±1.8
960	60	49°	1.40	1.166	14.03	9.32±0.44	1.59±0.10	4.71±0.22	1.48±0.05	136.4±4.8	63.9±2.1
960	100	49°	0.73	0.504	14.81	7.70±0.41	1.12±0.06	3.40±0.18	0.83±0.04	172.4±6.0	52.1±1.2
960	200	49°	0.24	0.148	15.94	9.26±0.39	0.62±0.04	4.26±0.18	0.74±0.03	242.1±8.5	15.5±0.4
969	20	47°		0.597	13.47	6.27±0.30	1.19±0.08	3.64±0.17	1.68±0.08	105.3±3.7	42.1±1.2
969	60	47°		1.166	13.70	6.18±0.30	1.19±0.08	2.56±0.12	1.13±0.06	132.2±4.6	62.8±1.8
969	100	47°		0.504	14.27	11.95±0.64	0.64±0.06	2.51±0.13	0.86±0.04	156.7±5.5	51.9±1.1
969	200	47°		0.148	15.10	7.95±0.33	0.38±0.04	4.54±0.18	0.48±0.03	223.8±7.8	16.7±0.5

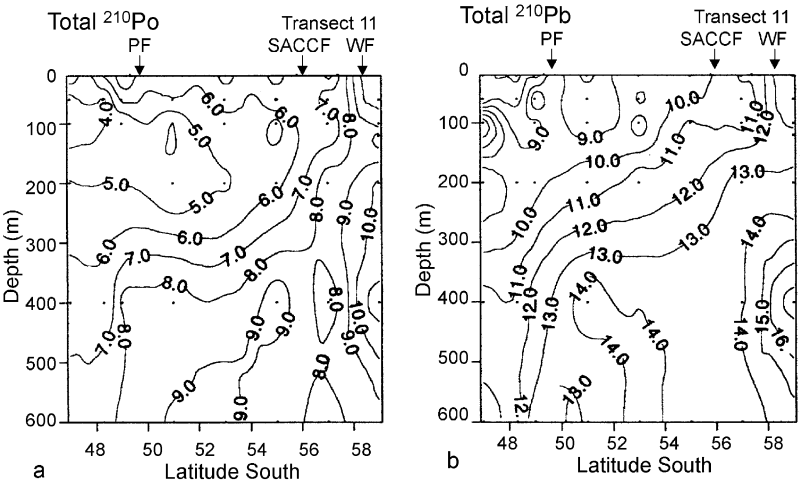

Fig. 2. Total activity (dissolved plus particulate) in dpm $100l^{-1}$ of (a) ^{210}Po and (b) ^{210}Pb in the water column, along the 6°W transect 11.

Farley and Turekian (1990). The distribution of ^{210}Po is different. Within the AASW, the Winter Water, identified by lower temperatures and higher salinities (Hellmer and Bersch, 1985), has lower ^{210}Po activity (4–6 dpm $100l^{-1}$). Advecting Upper Circumpolar Deep Water (UCDW) introduced higher activity (12–17 dpm ^{210}Pb $100l^{-1}$, 8–11 dpm ^{210}Po $100l^{-1}$) at the Weddell Front (WF) into the surface water.

The development of the phytoplankton bloom in the PFr and the retreat of the ice edge are reflected in the ^{210}Pb and ^{210}Po distribution. During all transects the ratio of total ^{210}Po/^{210}Pb in the mixed layer (Fig. 3) was mostly less than one. At the end of spring, during transect 11, near-equilibrium ratios were reached only in a very limited area at the Polar Front. The increase of phytoplankton density within the developing bloom was reflected by an increase of particulate ^{210}Po and ^{210}Pb. 25% of total ^{210}Po and 13% of total ^{210}Pb were adsorbed onto particles (Table 1). With the developing phytoplankton bloom in the PFr a conspicious ^{210}Po/^{210}Pb minimum of about 0.4–0.5 developed in the lower part of the euphotic zone, caused by a decrease in both dissolved and total ^{210}Po activity (Fig. 3). Below the euphotic zone, the ratio increased again to 0.6–0.7.

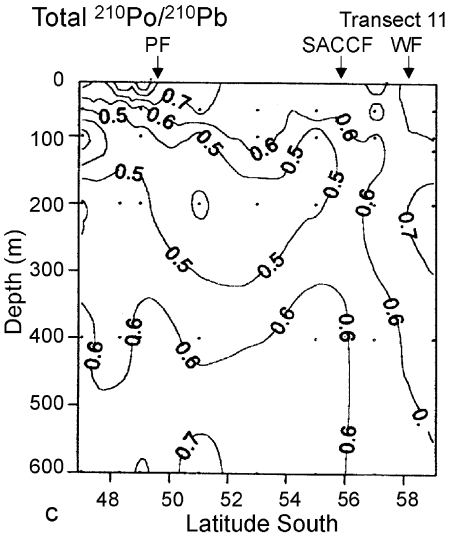

Fig. 3. ^{210}Po/^{210}Pb ratio of the total activity in transect 11 along 6°W.

3.1. Transect 2 (2 Oct–18 Oct)

At the beginning of spring, we observed near 55°S (Southern Antarctic Circumpolar Current Front, SACCF) between 60 and 200 m depth high activities of particulate ^{210}Pb and ^{210}Po (Fig. 4a

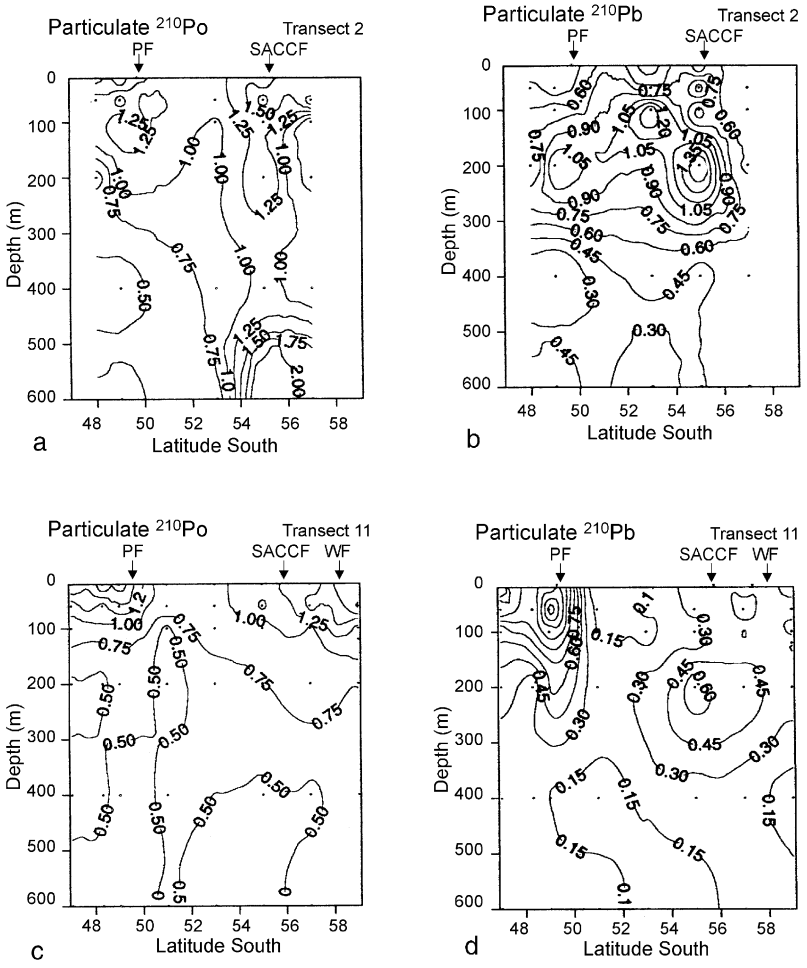

Fig. 4. Particulate ^{210}Po activity in dpm $100\,l^{-1}$ in transects (a) 2 and (c) 11 and particulate ^{210}Pb activity in dpm $100\,l^{-1}$ in transects (b) 2 and (d) 11 along 6°W.

and b). Bathmann et al. (1997) observed at this depth a maximum of empty diatom frustules of *Nitzschia prolongatoides*.

The Polar Front was located north of 50°30′S (Veth et al., 1997). An increase in chlorophyll *a* to about $0.55\,\mu g\,l^{-1}$ (Fig. 5a) together with a slight accumulation of particulate ^{210}Po and ^{210}Pb point to a developing phytoplankton bloom.

3.2. Transect 5 (22 Oct–30 Oct)

The ratio of ^{210}Po/^{210}Pb on particles increased from about 2 in transect 2 to >4 in the surface water of the southern ACC (Fig. 6a and b). Klaas (1997) observed a high proportion of non-siliceous organisms like heterotrophic microprotozoa (30–62%), which might be responsible for the particulate ^{210}Po/^{210}Pb ratio higher than in transect 2.

With increasing chlorophyll *a* concentration during the developing phytoplankton bloom in the PFr (Fig. 5b) a significantly higher amount of ^{210}Po and ^{210}Pb was adsorbed onto particles. Dissolved ^{234}Th was already depleted down to 70%, but total ^{234}Th was still near equilibrium with ^{238}U (Rutgers van der Loeff et al., 1997),

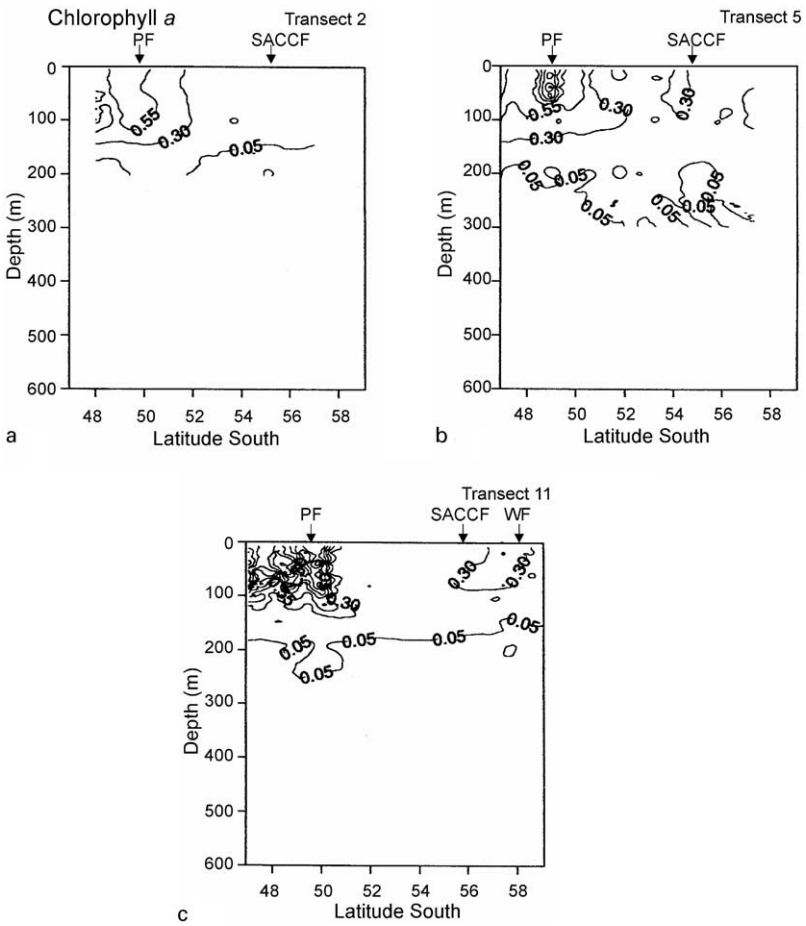

Fig. 5. Chlorophyll a in $\mu g\,l^{-1}$ in transects (a) 2, (b) 5 and (c) 11 along 6°W (data from Bathmann et al., 1997).

indicating that export of particles was still insignificant.

3.3. Transect 11 (10 Nov–21 Nov)

By the end of the spring, highest ^{210}Po and ^{210}Pb accumulations on particles were observed near the PF (Fig. 4c and d). Chlorophyll *a* concentrations of $>4\,\mu g\,l^{-1}$ (Fig. 5c, Bathmann et al., 1997) indicate well-developed phytoplankton blooms in the PFr. Three distinct blooms were detected, at 47°S and 48°30′S dominated by *Corethron criophilum*, at 49°S by *Corethron inerme* with high abundance of *Fragilariopsis kerguelensis* and at 50°S by *Fragilariopsis kerguelensis* with heavily silicified frustules (Bathmann et al., 1997). The $^{210}Po/^{210}Pb$ ratio of the particles of 1–2 shows slight excess of ^{210}Po (Fig. 6c). Highest particulate ^{210}Pb accumulation of about 13% of total activity was observed at about 49°S. The depletion of total ^{234}Th by up to 37% with respect to ^{238}U in the surface water ^{238}U (Rutgers van der Loeff et al., 1997) is due to beginning export of particulate matter out of the euphotic zone.

In the southern ACC the chlorophyll *a* concentrations remained unchanged at about $0.25\,\mu g\,l^{-1}$. In contrast to the situation at the PFr and the MIZ, in the sACC the ratio of particulate $^{210}Po/^{210}Pb$ rose to 8.

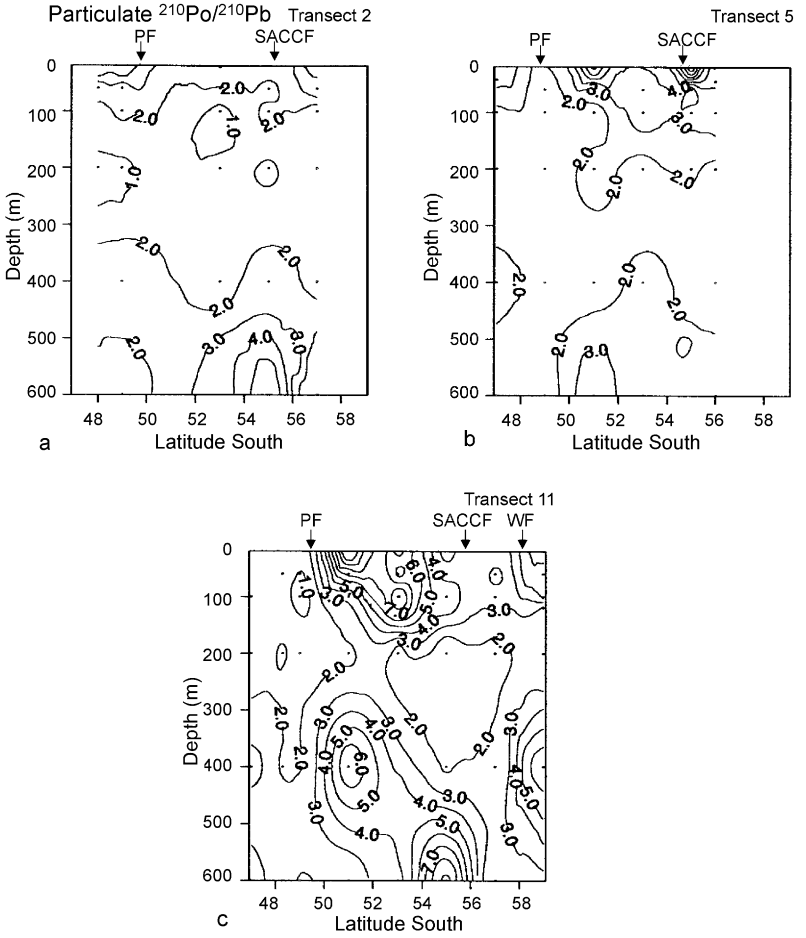

Fig. 6. $^{210}Po/^{210}Pb$ ratio of particles in transects (a) 2, (b) 5 and (c) 11.

4. Discussion

4.1. Non-steady-state scavenging model for ^{210}Po and ^{210}Pb

The affinity of ^{210}Pb and ^{210}Po for particles and especially for biogenic silica and POC, respectively, allows the use of these radionuclides for calculation of particle export rates from the surface water to depth. We intend to estimate POC and biogenic silica export from ^{210}Pb and ^{210}Po export for the short duration of several weeks of a phytoplankton bloom. During the development of the phytoplankton blooms in the PFr the plankton concentration and composition were changing very rapidly, and as a result the particulate radionuclide activities changed as well.

We now develop the non-steady-state solution for ^{210}Pb and ^{210}Po of the classical radionuclide-scavenging model of Bacon and Anderson (1982), and disregard advection and diffusion, for reasons discussed later

$$\frac{\partial A_{Pb}^{tot}}{\partial t} = A_{Ra}\lambda_{Pb} + I_{Pb} - A_{Pb}^{tot}\lambda_{Pb} - P_{Pb}, \quad (1)$$

$$\frac{\partial A_{Po}^{tot}}{\partial t} = A_{Pb}^{tot}\lambda_{Po} - A_{Po}^{tot}\lambda_{Po} - P_{Po}. \quad (2)$$

$A_{Pb}^{tot}$and A_{Po}^{tot} are the activities of total ^{210}Pb (dpm $100\,l^{-1}$) and total ^{210}Po (dpm $100\,l^{-1}$), A_{Ra} is the

activity of ^{226}Ra (dpm 100 l^{-1}), λ_{Pb} and λ_{Po} are the decay constants (day^{-1}) of ^{210}Pb and ^{210}Po, I_{Pb} is the ^{210}Pb input from the atmosphere, and P_{Pb} and P_{Po} are the export rates. The non-steady-state solution for ^{210}Pb is based on the model for ^{234}Th by Buesseler et al. (1992). We solve the Eqs. (1) and (2) for the non-steady-state case, assuming the fluxes P were constant during a period t between the sampling times t_1 and t_2 of two transects, with the corresponding activities A_1 and A_2.

$$A^{tot}_{Pb_2} = A_{Ra}(1 - e^{-\lambda_{Pb}t}) + A^{tot}_{Pb_1} e^{-\lambda_{Pb}t} + \frac{I_{Pb} - P_{Pb}}{\lambda_{Pb}}(1 - e^{-\lambda_{Pb}t}), \quad (3)$$

$$A^{tot}_{Po_2} = \frac{A_{Ra}\lambda_{Pb} + I_{Pb} - P_{Pb}}{\lambda_{Pb}} \times \left[\frac{\lambda_{Po}}{\lambda_{Po} - \lambda_{Pb}}(e^{-\lambda_{Po}t} - e^{-\lambda_{Pb}t}) + (1 - e^{\lambda_{Po}t})\right] + A^{tot}_{Pb_1}\frac{\lambda_{Po}}{\lambda_{Po} - \lambda_{Pb}}(e^{-\lambda_{Pb}t} - e^{-\lambda_{Po}t}) + A^{tot}_{Po_1} e^{-\lambda_{Po}t} - \frac{P_{Po}}{\lambda_{Po}}(1 - e^{\lambda_{Po}t}). \quad (4)$$

$A^{tot}_{Pb_1}$ and $A^{tot}_{Pb_2}$ are the total ^{210}Pb activities, $A^{tot}_{Po_1}$ and $A^{tot}_{Po_2}$ are the total ^{210}Po activities at the time t_1 and t. Rearranging (3) and (4) for the export flux P gives:

$$P_{Pb} = \lambda_{Pb}\left[\frac{A_{Ra}(1 - e^{-\lambda_{Pb}t}) + A^{tot}_{Pb_1} e^{-\lambda_{Pb}t} + \frac{I_{Pb}}{\lambda_{Pb}}(1 - e^{-\lambda_{Pb}t}) - A^{tot}_{Pb_2}}{(1 - e^{-\lambda_{Pb}t})}\right], \quad (5)$$

$$P_{Po} = \lambda_{Po}\left\{\frac{A_{Ra}\lambda_{Pb} + I_{Pb} - P_{Pb}}{\lambda_{Pb}}\left[\frac{\lambda_{Po}}{\lambda_{Po} - \lambda_{Pb}}(e^{-\lambda_{Po}t} - e^{-\lambda_{Pb}t}) + (1 - e^{-\lambda_{Po}t})\right] + A^{tot}_{Pb_1}\frac{\lambda_{Po}}{\lambda_{Po} - \lambda_{Pb}}(e^{-\lambda_{Pb}t} - e^{-\lambda_{Po}t}) + A^{tot}_{Po_1} e^{-\lambda_{Po}t} - A^{tot}_{Po_2}\right\}. \quad (6)$$

The non-steady-state export of ^{210}Pb and ^{210}Po, calculated with Eqs. (5) and (6), from the upper 100 m during the three transects is given in Table 2. The steady-state export is given for comparison.

Now we consider the influence of advection on the radionuclide distribution. Export calculations for a non-steady-state case are most useful if either the same water mass was sampled or an advection/diffusion term is included in the calculations. The meandering nature of the Polar Front, the southern ACC Front and the ACC Weddell Gyre boundary would require addition of advection and diffusion terms on the non-steady-state model. Since advection and diffusion values cannot be derived from the physical data gained during our expedition we have to rely on estimates only. Values for horizontal and vertical diffusion derived by Olbers and Wenzel (1989) show a large scatter in the ACC. Estimates from the buoyancy gradients using the relationship of Broecker (1981) cannot be applied, because this relationship is based on a system where the isopycnals run horizontally whereas in the ACC the isopycnals are inclined. Therefore, we have to rely on rough estimates of the influence of advection and diffusion to the radionuclide export calculations.

First, we consider vertical advection. Diapycnal diffusion is of minor importance since it is many orders of magnitude lower than isopycnal diffusion (Olbers and Wenzel, 1989). The upwelling of UCDW into the surface water between the SACCF and the WF with higher ^{226}Ra, ^{210}Pb and ^{210}Po activity has to be considered. Taking a vertical velocity of about 0.15×10^{-5} m s^{-1} along the Greenwich meridian between SACCF and WF (Gordon et al., 1977) and an activity of ^{210}Pb and ^{210}Po of the UCDW which is about 30 dpm m^{-3}

Table 2
Integrated export of ^{210}Pb (dpm m^{-2} d^{-1}) and ^{210}Po (dpm m^{-2} d^{-1}) from the upper 100 m as a function of latitude, calculated with the non-steady-state (NSS) and steady-state model (SS). Negative values indicate input of activity

Lat. (°S)	Stations in transect			Depth (m)	P_{Pb} Export NSS (dpm m^{-2} d^{-1})		P_{Po} Export NSS (dpm m^{-2} d^{-1})		P_{Pb} Export SS (dpm m^{-2} d^{-1})		P_{Po} Export SS (dpm m^{-2} d^{-1})	
	2	5	11		2–5	5–11	2–5	5–11	2	11	2	11
56.5	868	886	941	100	252	−76	-22	61	8	6	22	21
55	872	891	945	100	117	−47	195	32	6	6	11	22
53	876	895	949	100	123	−13	0	54	14	2	19	17
51		899	953	100		14		19		2		16
49	877	903	960	100	101	−31	145	11	4	15	1.41	16
47.5	879	907	969	60[a]	−1.8	50	−5.4	71	4	17	−0.05	19
47.5		907	969	100		4		107		21		25

[a] 100 m value of station 879 is missing. Stations at 47 and 48°S and stations at 56 and 57°S have been put into two categories named 47.5 and 56.5°S.

higher than in the AASW, the advective input into the surface water would amount to about 4 dpm m^{-2} d^{-1}. This implies an influence on ^{210}Po export (Table 2, non-steady-state export during transects 5–11) of 7–13%.

Second, we consider the south-north advection of the AASW. From volume transport of 21.5 Sv of AASW to the north and a surface-water depth of 120 m (Keir, 1988) follows a transport velocity to the north of roughly 0.55 km d^{-1} at 50°S. In the 35 days between the first and the last transect of our expedition the surface water has traveled 20 km to the north. With an activity gradient of about 0.1 dpm m^{-3} km^{-1} for ^{210}Po and ^{210}Pb the activity input by south-north advection of AASW amounts to approximately 7 dpm m^{-2} day^{-1}. This is about 37% of the ^{210}Po export and 50% of the ^{210}Pb export at 51°S (Table 2, non-steady-state export during transects 5–11).

We realize, neglecting advection in the ACC implies to assume constant radionuclide concentrations and fluxes along the path of the ACC. In reality, the ^{210}Pb and the ^{210}Po distribution is formed by export processes over a large area. The geostrophic speed of the ACC is approximately 30 cm s^{-1} in the high-speed core of the Polar Front (Whitworth and Nowlin, 1987). By means of the eastward flow of the ACC, the disequilibrium of ^{210}Po and ^{210}Pb, measured at 6°W, is a result of export, decay and production during a 3500 km transit during the half-life of ^{210}Po (distance between half-life arrow and investigation area in Fig. 1). The possibility of zonal variability causes appreciable uncertainty, especially in the case of the long-lived isotope ^{210}Pb.

4.2. Affinity of ^{210}Po and ^{210}Pb for POC and biogenic silica

In the open ocean, the particles that scavenge and remove ^{210}Pb and ^{210}Po from the water column consist mainly of organic matter, e.g. biodetritus, organic and inorganic colloids and plankton. The depletion of total ^{210}Pb with respect to ^{226}Ra and of ^{210}Po with respect to total ^{210}Pb in the surface water is caused by the removal with larger, sinking particles. The adsorption rate of a radionuclide is dependent on its physico-chemical behavior, its concentration in the water, the particle concentration and particle composition in the water. Kharkar et al. (1976) and Heyraud et al. (1976) found the following relative adsorption intensities:

$$\mathrm{Po} \gg \mathrm{Pb} = \mathrm{Th} \gg \mathrm{Ra} > \mathrm{U}.$$

Several authors reported differences in the bioaccumulation of ^{210}Pb and ^{210}Po. Fisher et al. (1983) showed in culture experiments, that ^{210}Pb appears to associate almost exclusively with structural components (cell walls and plasmalemmae) of diatoms and shows no evidence of protein association, i.e. material not easily assimilated by

herbivorous zooplankton. In contrast, ^{210}Po associates with cellular organic compounds. The cellular distribution of ^{210}Po is more uniform in naked flagellates and in general follows more closely the protein distribution (Fisher et al., 1983). They conclude that the bioaccumulation of ^{210}Pb and ^{210}Po proceeds passively via adsorption onto cell surfaces. Once ^{210}Po is associated with certain proteins along a cell membrane, it may be carried into the interior of the cell. Erleksova (1960) already reported the formation of Po-protein complexes. Therefore, it can be expected that ^{210}Po would be assimilated to a greater extent by herbivorous plankton than ^{210}Pb. The herbivores graze on algae and accumulate the algal protein containing the ^{210}Po. We found that *Salpa thompsoni* within the sACC incorporated up to 25 dpm ^{210}Po per individual, corresponding to phytoplankton-Po of 2.5 m^3 seawater. This does not affect ^{210}Pb, as salps had a ^{210}Pb content of only 1 dpm per individual, which would correspond to the particulate fraction of about 200 l seawater. Most of the ^{210}Pb that is bound to the cell walls is excreted with the feces. This is consistent with data reported by Shannon et al. (1970), Kharkar et al. (1976), Beasley et al. (1978) and Heyraud and Cherry (1979), which indicated high ^{210}Po/^{210}Pb ratios in various plankton species. Fisher et al. (1983) concluded that ^{210}Po/^{210}Pb ratios in fecal pellets of zooplankton are half those of their phytoplankton food supply in field samples. In addition, Ritchie and Shimmield (1991) and Miquel et al. (1993) refer to the role of fecal pellets in transporting radionuclides from the surface water to depth.

It is likely that part of Po is accumulated with free-living bacteria in the colloidal fraction, since they consist of the material onto which Po preferably adsorbs. During our investigation, a low percentage of phytoplankton biomass was converted to bacterial biomass; thus carbon that does not leave the surface water. Bacterial production was on average 8% of primary production in the PFr and 20% in the southern ACC (Lochte et al., 1997). Since we aim to trace the export of C and BSi with larger sinking particles, it does not much affect our budget.

In our study, the change in the phytoplankton composition towards dominance of siliceous plankton (97% phytoplankton carbon of diatoms and only 3% phytoplankton carbon of flagellates at 48°45′S, Bathmann et al., 1997) during the development of the blooms in the PFr was reflected by a decreasing particulate ^{210}Po/^{210}Pb ratio. We interpret this as a result of preferential adsorption of ^{210}Pb onto siliceous frustules. In contrast, in the upper 100 m of the southern ACC, 30–62% of microprotist plankton biomass consisted of heterotrophs (Klaas, 1997), non-siliceous organisms. Here we found high particulate ^{210}Po/^{210}Pb ratios. These heterotrophs presumably accumulated ^{210}Po by grazing on algae, incorporating the ^{210}Po whereas ^{210}Pb was excreted. Peeken (1997) distinguished at transect 11 a higher diatom abundance of about 50–60% in the southern ACC (54–55°S and 57°30′S). Here we found low particulate ^{210}Po/^{210}Pb ratios of about 2–3 (Fig. 6).

Plotting the particulate ^{210}Po/^{210}Pb ratio as a function of POC (Fig. 7a) and biogenic silica (Fig. 7b) illustrates the preference of ^{210}Po for POC and of ^{210}Pb for biogenic silica. In the southern ACC, the biomass remained low throughout the spring with a dominance of non-siliceous plankton resulting in low POC concentrations and low biogenic silica concentrations but high particulate ^{210}Po/^{210}Pb ratios. Regardless of the low POC concentrations the particles adsorbed relatively much ^{210}Po but little ^{210}Pb, resulting in particulate ^{210}Po/^{210}Pb ratios of 4–12. With increasing chlorophyll *a* concentrations during the development of the phytoplankton blooms at the PFr, the concentration of biogenic silica increased because of increasing diatom abundance. Hence, more ^{210}Pb is adsorbed onto the silica frustules. More ^{210}Po is adsorbed as well, but the ^{210}Po/^{210}Pb ratio of the particles remains low, about 1–2. Low POC/BSi ratios cause low ^{210}Po/^{210}Pb ratios, as shown in Fig. 7c.

We therefore conclude that the ^{210}Po and ^{210}Pb accumulation depend not only on particle concentration but also on particle composition. We will now test the use of ^{210}Po as tracer for POC and of ^{210}Pb and ^{234}Th as better tracer for biogenic silica to characterize the nature of particles settling

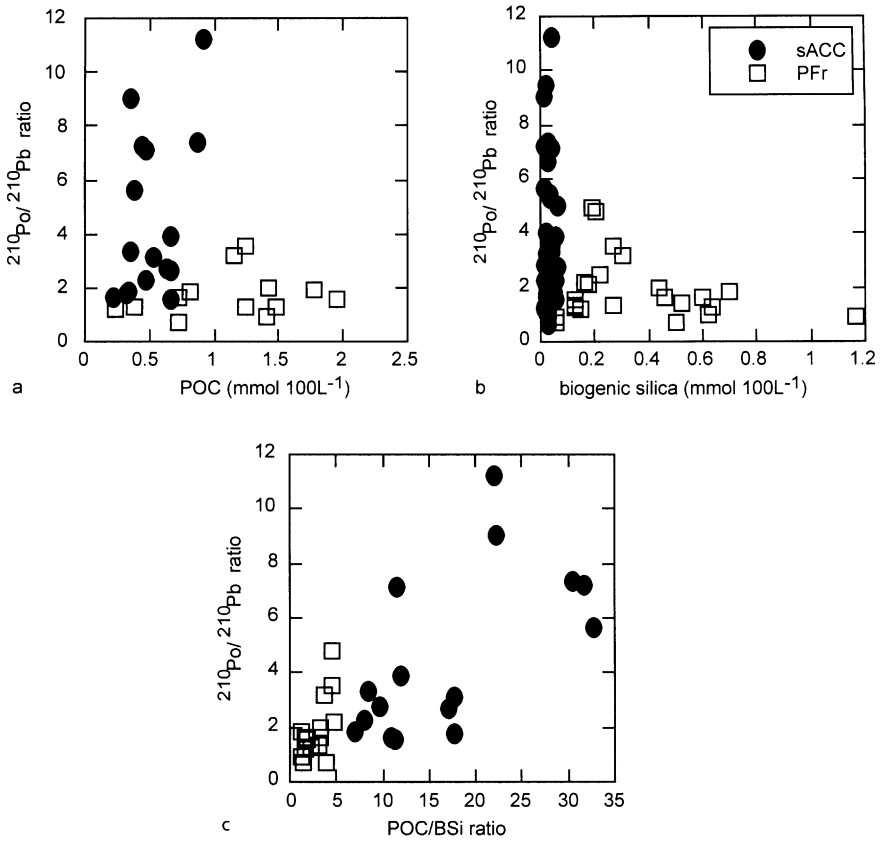

Fig. 7. Particulate ^{210}Po/^{210}Pb ratio as a function of (a) POC and (b) biogenic silica and (c) POC/BSi ratio.

out of the euphotic zone during the phytoplankton bloom in the PFr.

4.3. POC and biogenic silica export in the PFr

We propose that it is possible to distinguish between POC and biogenic silica export if we use two tracers with different affinities. We base the two-tracer model on the assumption that adsorption of a particle-reactive radionuclide is determined by the composition of the particles. In the case of a diatom bloom, the particles consist mostly of biogenic silica and POC. Using multiple regression equations of all samples in the PFr and the sACC from 0 to 200 m ($n = 31$) we can show, that, in agreement with literature, ^{210}Po has a strong preference for POC over BSi, which is very distinct from the affinities of both ^{234}Th and ^{210}Pb. The multiple regression equations are

$$A_{\mathrm{Po}}^{\mathrm{part}} = A_{\mathrm{Po}}^{\mathrm{diss}}(a_1\mathrm{POC} + b_1\mathrm{BSi}), \quad (7)$$

$$A_{\mathrm{Pb}}^{\mathrm{part}} = A_{\mathrm{Pb}}^{\mathrm{diss}}(a_2\mathrm{POC} + b_2\mathrm{BSi}), \quad (8)$$

$$A_{\mathrm{Th}}^{\mathrm{part}} = A_{\mathrm{Th}}^{\mathrm{diss}}(a_3\mathrm{POC} + b_3\mathrm{BSi}), \quad (9)$$

where $A_{\mathrm{Po}}^{\mathrm{part}}$ is the particulate ^{210}Po activity, $A_{\mathrm{Po}}^{\mathrm{diss}}$ the dissolved ^{210}Po activity, a_1 and b_1 the coefficients of multiple regression, and POC and BSi the concentrations of particulate organic carbon and biogenic silica. This was written in a similar way for ^{210}Pb with the coefficients a_2 and b_2 in Eq. (8), and for ^{234}Th with a_3 and b_3 in Eq. (9). The regression analysis (Table 3) confirms that ^{210}Po is strongly related to POC but not to BSi, whereas ^{210}Pb and ^{234}Th are related to both POC and BSi. Based on Table 3, we now select the

Table 3
Results of multiple regression of the particulate/dissolved ratio of the tracers ^{210}Po, ^{210}Pb and ^{234}Th as function of POC and BSi content of the particles of all sACC and PFr stations ($n = 31$). Given is the regression coefficient associated with each independent variable; SE = standard error of the regression coefficient. The associated probability P is given for each variable

	Coef.	±SE	Coef. $-P$	R^2
^{210}Po				
POC	a_1 0.291	±0.031	<0.001	0.89
BSi	b_1 −0.053	±0.075	0.487	
^{210}Pb				
POC	a_2 0.047	±0.01	<0.001	0.88
BSi	b_2 0.108	±0.025	<0.001	
^{234}Th				
POC	a_3 0.138	±0.019	<0.001	0.94
BSi	b_3 0.246	±0.045	<0.001	

tracer pairs that have different affinities for POC and BSi. Apart from the tracer pair ^{210}Po–^{210}Pb we use the tracer pair ^{210}Po–^{234}Th. Like ^{210}Pb, ^{234}Th is strongly bound to particle surfaces. The advantage of ^{234}Th over ^{210}Pb is its relatively short half-life, which causes its distribution to represent a far shorter scavenging history. The scatter in the ^{234}Th-based export flux is therefore considerably smaller than in fluxes based on ^{210}Pb, as already discussed.

Having expressed the particulate radionuclide concentrations as a function of POC and BSi contents, we now assume that POC and BSi settle with the adsorbed radionuclides, each at a characteristic sinking velocity of s_{POC} and s_{BSi}, respectively. The export flux P of ^{210}Po, ^{210}Pb and ^{234}Th out of the euphotic zone can now be described as

$$P_{Po} = A_{Po}^{diss}(a_1 s_{POC}\mathrm{POC} + b_1 s_{BSi}\mathrm{BSi}), \quad (10)$$

$$P_{Pb} = A_{Pb}^{diss}(a_2 s_{POC}\mathrm{POC} + b_2 s_{BSi}\mathrm{BSi}), \quad (11)$$

$$P_{Th} = A_{Th}^{diss}(a_3 s_{POC}\mathrm{POC} + b_3 s_{BSi}\mathrm{BSi}). \quad (12)$$

In earlier studies, based on only one tracer, it was noticed that the ratio of tracer to POC content was different in suspended and sinking material (a problem discussed in Buesseler et al., 2000 and Rutgers van der Loeff et al., submitted). In our study, we explicitly allow here differential settling of two flux components, which may explain part of the observed differences in composition between suspension and sinking flux. We do not apply the 30–60% reduction of the POC/^{234}Th ratio in surface water suspended matter used for the export estimate by Rutgers van der Loeff et al. (1997).

The combination of two tracers with different affinities for POC and biogenic silica, i.e. ^{210}Po and ^{210}Pb, ^{210}Po and ^{234}Th, yields the ratio of the radionuclide export flux

$$\frac{P_{Po}}{P_{Pb}} = \frac{\frac{A_{Po}^{diss}}{A_{Pb}^{diss}}\left(a_1\frac{s_{POC}}{s_{BSi}}\frac{\mathrm{POC}}{\mathrm{BSi}} + b_1\right)}{\left(a_2\frac{s_{POC}}{s_{BSi}}\frac{\mathrm{POC}}{\mathrm{BSi}} + b_2\right)}, \quad (13)$$

$$\frac{P_{Po}}{P_{Th}} = \frac{\frac{A_{Po}^{diss}}{A_{Th}^{diss}}\left(a_1\frac{s_{POC}}{s_{BSi}}\frac{\mathrm{POC}}{\mathrm{BSi}} + b_1\right)}{\left(a_3\frac{s_{POC}}{s_{BSi}}\frac{\mathrm{POC}}{\mathrm{BSi}} + b_3\right)}. \quad (14)$$

Re-arranging Eqs. (13) and (14) yields the ratio of the sinking velocities, i.e. the preferential settling of BSi or POC

$$\frac{s_{BSi}}{s_{POC}} = \frac{\frac{\mathrm{POC}}{\mathrm{BSi}}\left(a_1\frac{A_{Po}^{diss}}{A_{Pb}^{diss}} - a_2\frac{P_{Po}}{P_{Pb}}\right)}{\left(b_2\frac{P_{Po}}{P_{Pb}} - b_1\frac{A_{Po}^{diss}}{A_{Pb}^{diss}}\right)}, \quad (15)$$

$$\frac{s_{BSi}}{s_{POC}} = \frac{\frac{\mathrm{POC}}{\mathrm{BSi}}\left(a_1\frac{A_{Po}^{diss}}{A_{Th}^{diss}} - a_3\frac{P_{Po}}{P_{Th}}\right)}{\left(b_3\frac{P_{Po}}{P_{Th}} - b_1\frac{A_{Po}^{diss}}{A_{Th}^{diss}}\right)}. \quad (16)$$

The radionuclide data in Table 4 (^{234}Th export from Rutgers van der Loeff et al., 1997) and the correlation coefficients listed in Table 3 are used in Eqs. 15 and 16 to estimate the ratio of the sinking velocities of BSi and POC, which we call the BSi sinking preference (Table 4). We have shown that export has to be calculated with a non-steady state equation. This implies that we need two consecutive stations at approximately the same position.

Table 4
Representative values for the PFr and the sACC, obtained from averages of all data (0–200 m). Data of stations at 56.5°S, 55°S, 53°S, 51°S, 49°S and 47°S were applied to Eqs. (15) and (16) to calculate the BSi sinking preference. Coefficients of multiple regressions are taken from Table 3. Sinking velocities and corresponding POC and BSi export were derived from Eqs. (10) and (12) using the $^{210}Po/^{234}Th$ tracer pair

Water column data (dpm $100l^{-1}$)	PFr	sACC
$^{210}Po_{dissolved}$	4.63	4.98
$^{210}Pb_{dissolved}$	8.54	9.69
$^{234}Th_{dissolved}$	180.80	208.90
POC, BSi in suspension (mmol $100l^{-1}$)		
POC	0.91	0.52
BSi	0.39	0.04

Export data ($dpm\,m^{-2}\,d^{-1}$)							
Latitude South	47°S	47°S	49°S	51°S	53°	55°	56.5°
Stations	907–969	907–969	903–960	899–953	895–949	891–945	886–941
Depth interval	0–60 m	0–100 m	0–100 m	0–100 m	0–100 m	0–100 m	0–100 m
$^{210}Po_{export}$	71	107	11	19	54	32	61
$^{210}Pb_{export}$	50	4	−31	14	−13	−47	−76
$^{234}Th_{export}$	2634	3250	1790	1700	1210	1300	160
BSi sinking preference							
Using ^{210}Po and ^{210}Pb	1.17	−0.88	−42.45	6.42	−10.64	−50.98	−40.96
Using ^{210}Po and ^{234}Th	1.09	0.72	5.37	17.48	0.83	6.29	−6.25
Sinking velocities ($m\,d^{-1}$)							
$BSi_{sinking\ velocity}$	6.9	6.6	8.3	58.4	6.0	29.3	−46.5
$POC_{sinking\ velocity}$	6.3	9.2	1.5	3.3	7.2	4.7	7.4
POC and BSi export ($mmol\,m^{-2}\,d^{-1}$)							
BSi_{export}	26.91	25.88	32.36	23.34	2.40	11.71	−18.60
POC_{export}	57.60	84.13	14.06	17.36	37.70	24.21	38.71
BSi_{export} in 22 days ($mol\,m^{-2}$)	0.59	0.57	0.71	0.51	0.05	0.26	−0.41
POC_{export}	1.27	1.85	0.31	0.38	0.83	0.53	0.85

Since appreciable export took place only in the period between transect 5 and 11, as derived from the ^{234}Th results, we select the station pairs 907–969 and 903–960 in the PFr, and 899–953, 895–949, 891–945, 886–941 in the southern ACC.

The large errors in the Pb-based export fluxes, associated with its long half-life, lead to unrealistic results (negative export ratios, Table 4) and preclude the use of ^{210}Pb as a reliable export tracer in the ACC. Applying the tracer pair ^{210}Po–^{234}Th, we obtain little preferential settling of biogenic silica at the different depth ranges at 47°S (station 969), although Crawford et al. (1997) observed a mass sinking of the diatom *Corethron inerme* at 48°S. However, Crawford et al. (1997) used for their study multinet hauls from 25 m depth to the surface, whereas our calculations are based on samples from 20 to 200 m depth. It is possible that the empty frustules of *Corethron* were sinking out from the very surface but were recycled in the water column below. Since *Corethron* species are rare in the sediments, despite their abundance in the water column, one possible fate might be recycling in the water column. Crawford et al. (1997) state further that the chlorophyll and

phytoplankton distribution data indicate an assemblage more or less equally composed of pelagic diatoms and flagellates north of 48°30′S. Both components settle apparently at about the same rate. In contrast, at station 960 at 49°S, a distinct preference of BSi settling was observed. At this station, heavily silicified frustules of *Fragilariopsis kerguelensis* were observed (Bathmann et al., 1997). Quéguiner et al. (1997) found 80% of the diatom cells composed by *Fragilariopsis kerguelensis* and roughly half of that empty. They further report an uncoupling of the BSi and POC concentration between the surface and 100 m depth: POC values were maximum in the surface while the BSi profile followed the Chl *a*. These evidences suggest a senescent population sinking out of the surface water. At this station, we found the highest BSi and lowest POC export flux within the PFr (Table 4). Our results support the observations of Quéguiner et al. (1997), and demonstrate how selective our two-tracer approach models the particle flux within phytoplankton blooms.

In the southern ACC, although the suspended particulate matter did not consist mainly of siliceous organisms (Quéguiner et al., 1997), we found a preferential settling of siliceous material over POC at 51°S and 55°S (Table 4). At 55°S, about 40% of the phytoplankton consisted of diatoms (Peeken, 1997). Such a preferential settling of BSi might result from the growth of heavily silicified diatoms under iron stress (Hutchins and Bruland, 1998). We note, however, that communities with heaviliy silicified diatoms were observed in the north, not in the southern ACC (Bathmann et al., 1997). It seems reasonable to assume, that if any export occurs in the southern ACC, it is related to diatoms. In contrast, we found no settling preference of BSi at 53°S. We relate this to the mass occurrence of salps at this latitude (Dubischar and Bathmann, 1997). Since salps accumulate huge amounts of ^{210}Po but less ^{234}Th (Friedrich, 1997), the ^{210}Po, hence POC, seems to be exported. The salps are not included in the particulate fraction, since they are not caught with our GERARD bottles. We cannot explain the negative export ratios at 56.5°S resulting from the high ^{210}Po export and the low ^{234}Th export.

The export flux of POC and BSi (Table 4) was derived from Eqs. (10) and (12), applying our simple approximation mentioned above, i.e. that flux equals the sinking velocity times particle concentration. The export from the mixed layer in the PFr during a 22-day period amounted to 0.3–1.85 mol POC m^{-2} and 0.6–0.7 mol BSi m^{-2}. In the southern ACC, the POC export (0.4–0.8 mol m^{-2}) was less than half of the value in the PFr, whereas the export of biogenic silica ranged between 0.05 and 0.5 mol m^{-2} for the same period. These results would suggest that the BSi flux in the southern ACC is not homogeneous and is on average lower than during a bloom in the PFr. We cannot exclude, that inhomogeneities in the flux results are due to uncertainties in the ^{210}Po and the ^{234}Th fluxes. The export fluxes in the non-steady-state model are based on the difference between two successive profiles. In the southern ACC, these differences were relatively low, and the export rates have a correspondingly high error. The neglect of an advective term adds another uncertainty to the fluxes, especially to the calculated export of the longer-lived ^{210}Po (Fig. 7). In the PFr, the fluxes are higher and the derived BSi and POC fluxes are consequently more robust. It has been our aim to demonstrate how these two radionuclides can be used to distinguish between the export rates of the two major components of the flux: POC and biogenic silica. The method will be more powerful in an area where advection is less important or where it can be properly accounted for. In that case, the application of the other tracer pair, ^{210}Po–^{210}Pb, might be again a possible alternative.

Now we compare our estimates of carbon export in the PFr to the other components of the carbon budget of the phytoplankton bloom. Primary production, derived from ^{14}C incubations, produced 2.5 mol C m^{-2} during a 22-day period (Jochem et al., 1995). Net CO_2 incorporation in biomass (production minus mineralization), estimated from measurements of the carbonate system, was 1.1 mol C m^{-2} during the same 22-day period (Bakker et al., 1997). POC export for the 22-day period, derived from our ^{210}Po–^{234}Th tracer model, amounts, on average, to 1.15 mol C m^{-2} or 46% of the ^{14}C estimated

primary production. This export corresponds well with the annual carbon flux of 1.27 mol m^{-2} at 100 m derived from sediment trap studies (Wefer and Fischer, 1991), which occurs only during a short period of the year.

Production estimates of biogenic silica in the PFr, obtained from Si/C ratio, are 0.29–1.25 mol m^{-2} for the 22-day period, between transect 5 and 11 (Quéguiner et al., 1997). Biogenic silica export from the mixed layer, derived from our ^{210}Po–^{234}Th tracer approach, was 0.62 mol m^{-2}, on average. According to our estimate, 200 to 50% of the biogenic silica production would have been exported from the mixed layer in the PFr during the phytoplankton bloom in October/November 1992.

Acknowledgements

We are grateful to the crew of R/V *Polarstern* and the chief scientist of the SO-JGOFS cruise Victor Smetacek. We further thank the oceanography team of Cornelis Veth for providing the hydrographical and transmissometer data, Heike Höltzen for the help with GERARD sampling and radionuclide analysis, Corinna Dubischar and Ulrich Bathmann for the POC data, Bernard Quéguiner for the biogenic silica data and Knut Heier for the help with mathematics. The helpful comments by Michael P. Bacon and one anonymous reviewer appreciably improved the manuscript. This is an AWI contribution no. awi-n10119.

References

Anderson, R.F., Fleer, A.P., 1982. Determination of natural actinides and plutonium in marine particulate material. Analytical Chemistry 54, 1142–1147.

Bacon, M.P., Anderson, R.F., 1982. Distribution of thorium isotopes between dissolved and particulate forms in the deep sea. Journal of Geophysical Research 87 (C3), 2045–2056.

Bacon, M.P., Spencer, D.W., Brewer, P.G., 1976. ^{210}Po/^{210}Ra and ^{210}Po/^{210}Pb disequilibria in seawater and suspended particulate matter. Earth and Planetary Science Letters 32, 277–296.

Bakker, D.C.E., de Baar, H.J.W., Bathmann, U.V., 1997. Changes of carbon dioxide in surface waters during spring in the Southern Ocean. Deep-Sea Research II 44, 91–127.

Bathmann, U.V., Scharek, R., Klaas, C., Dubischar, C.D., Smetacek, V., 1997. Spring development of phytoplankton biomass and composition in major water masses of the Atlantic sector of the Southern Ocean in spring. Deep-Sea Research II 44, 51–67.

Beasley, T.M., Heyraud, M., Higgo, J.J.W., Cherry, R.D., Fowler, S.W., 1978. ^{210}Po and ^{210}Pb in Zooplankton Fecal Pellets. Marine Biology 44, 325–328.

Broecker, W.S.,1981. Geochemical tracers and ocean circulation. In: Warren, B.A., Wunsch, C. (Eds.) Evolution of Physical Oceanography. 459–460.

Buesseler, K.O., Bacon, M.P., Cochran, J.K., Livingston, H.D., 1992. Carbon and nitrogen export during the JGOFS North Atlantic bloom experiment estimated from ^{234}Th: ^{238}U disequilibria. Deep-Sea Research 39, 1115–1137.

Buesseler, K.O., Andrews, J.A., Hartman, M.C., Belastock, R., Chai, F., 1995. Regional estimates of the export flux of particulate organic carbon derived from ^{234}Th during the JGOFS EqPac program. Deep-Sea Research II 42, 777–804.

Buesseler, K.O., Ball, L., Andrews, J., Benitez-Nelson, C., Belastock, R., Chai, F., Chao, Y., 2000. Upper ocean transport of particulate organic carbon in the Arabian Sea derived from ^{234}Th. Deep-Sea Research II 45, 2461–2487.

Cherry, R.D., Fowler, S.W., Beasley, T.M., Heyraud, M., 1975. Polonium-210: Its vertical oceanic transport by zooplankton metabolic activity. Marine Chemistry 3, 105–110.

Craig, H., Krishnaswami, S., Somayajulu, B.L.K., 1973. ^{210}Pb-^{226}Ra: Radioactive disequilibrium in the deep sea. Earth and Planetary Science Letters 17, 295–305.

Crawford, R.M., Hinz, F., Rynearson, T., 1997. Spatial and temporal distribution of assemblages of the diatom *Corethron criophilum* in the polar frontal region of the South Atlantic. Deep-Sea Research II 44, 457–478.

Dubischar, C.D., Bathmann, U.V., 1997. Grazing impact of copepods and salps on phytoplankton in the Atlantic sector of the Southern Ocean. Deep-Sea Research II 44, 415–433.

Erleksova, E.V., 1960. Distribution of radioaktive elements in the animal organism. Israel program for Scientific translation, 161 pp., cited in Bennett, J.T., Carpenter, R. (1979) concentrations and temporal variations of ^{210}Po ^{210}Pb and Al in the Surf Zone Ecosystem of Copalis Beach, Washington. Estuarine and Coastal Marine Science 8, 127–140.

Farley, K.A., Turekian, K.K., 1990. Lead-210 in the circumpolar south atlantic. Deep-Sea Research 37 (12), 1819–1860.

Fischer, G., Fütterer, D., Gersonde, D.R., Honjo, S., Ostermann, D., Wefer, G., 1988. Seasonal variability of particle flux in the Weddell Sea and its relation to ice cover. Nature 335, 426–428.

Fisher, N.S., Burns, K.A., Cherry, R.D., Heyraud, M., 1983. Accumulation and cellular distribution of ^{241}Am, ^{210}Po and ^{210}Pb in two marine algae. Marine Ecology Progress Series 11, 233–237.

Fisher, N.S., Cochran, J.K., Krishnaswami, S., Livingston, H.D., 1988. Predicting the Oceanic flux of radionuclides on sinking biogenic debris. Nature 335, 622–625.

Fleer, A.P., Bacon, M.P., 1984. Determination of ^{210}Po and ^{210}Pb in seawater and marine particulate matter. Nuclear Instruments and Methods in Physics Research 223, 243–249.

Flynn, W.W., 1968. The determination of low levels of polonium-210 in environmental materials. Analytica Chimica Acta 43, 221–227.

Friedrich, J., 1997. Polonium-210 and Lead-210 in the Southern Polar Ocean: naturally occurring tracers of biological and hydrographical processes in the surface waters of the Antarctic circumpolar current and the Weddell Sea. Berichte zur Polarforschung 235, 1–155 (in German).

Gardner, W.D., Walsh, I.D., Richardson, M.J., 1993. Biophysical forcing of particle production and distribution during a spring bloom in the North Atlantic. Deep-Sea Research II 40, 171–195.

Gordon, A.L., Taylor, H.W., Georgi, D.T., 1977. Antarctic oceanographic zonation. In: Dunbar, M.J. (Ed.), Polar Oceans. Arctic Institute of North America, pp. 45–67.

Hellmer, H.H., Bersch, M., 1985. The Southern Ocean—A survey of oceanographic and marine meteorological research work. Berichte zur Polarforschung, 26.

Heyraud, M., Cherry, R.D., 1979. Polonium-210 and lead-210 in marine food chains. Marine Biology 25, 227–236.

Heyraud, M., Fowler, S.W., Beasley, T.M., Cherry, R.D., 1976. Polonium-210 in euphausiids: a detailed study. Marine Biology 34, 127–138.

Hutchins, D.A., Bruland, K.W., 1998. Iron-limited diatom growth and Si:N uptake ratios in a coastal upwelling regime. Nature 393, 561–564.

Jochem, F.J., Mathot, S., Quéguiner, B., 1995. Size-fractionated primary production in the open Southern Ocean in austral spring. Polar Biology 15, 381–392.

Keir, R.S., 1988. On the late Pleistocene ocean geochemistry and circulation. Paleoceanography 3, 413–445.

Kharkar, D.P., Thomson, J., Turekian, K.K., Forster, W.O., 1976. Uranium and thorium decay series nuclides in plankton from the Caribbean. Limnology and Oceanography 21, 294–299.

Klaas, C., 1997. Microzooplankton distribution and grazing impact in the Antarctic circumpolar current. Deep-Sea Research II 44, 375–393.

Ku, T.-L., Lin, M.-Ch., 1976. ^{226}Ra distribution in the Antarctic Seawater. Earth and Planetary Science Letters 32, 236–248.

Lochte, K., Bjornsen, P.K., Giesenhagen, H., Weber, A., 1997. Bacterial standing stock and production and their relation to phytoplankton in the Southern Ocean. Deep-Sea Research II 44, 321–340.

Miquel, J.C., Heyraud, M., Cherry, R.D., 1993. ^{210}Pb as a dietary indicator in the Antarctic pelagic community. Marine Biology 111, 161–171.

Moore, W.S., Dymond, J., 1988. Correlation of ^{210}Pb removal with organic carbon fluxes in the Pacific Ocean. Nature 331, 339–341.

Murray, J.W., Downs, J.N., Strom, S., Wei, C.-L., Jannasch, H.W., 1989. Nutrient assimilation, export production and ^{234}Th scavenging in the eastern equatorial Pacific. Deep-Sea Research 36, 1471–1489.

Nozaki, Y., Tsunogai, S., 1976. ^{226}Ra, ^{210}Pb and ^{210}Po disequilibria in the western North Pacific. Earth and Planetary Science Letters 32, 313–321.

Olbers, D., Wenzel, M., 1989. Determining diffusivities from hydrographic data by inverse methods with applications to the Circumpolar Current. In: Anderson, D.L.T., Willebrand, J. (Eds.), Oceanic Circulation Models: Comining Data and Dynamics. Kluwer Academic Publishers, Dordrecht, pp. 95–139.

Peeken, I., 1997. Photosynthetic pigment fingerprints as indicator of phytoplankton biomass and development in different water masses of the Southern Ocean during austral spring. Deep-Sea Research II 44, 261–282.

Peterson, R.G., Stramma, L., 1991. Upper-level circulation in the South Atlantic Ocean. Progress and Oceanography 26, 1–73.

Quéguiner, B., Tréguer, P., Peeken, I., Scharek, R., 1997. Biogeochemical dynamics and the silicon cycle in the Atlantic sector of the Southern Ocean during austral spring 1992. Deep-Sea Research II 44, 69–89.

Rama, M., Koide, Goldberg, D.E., 1961. ^{210}Pb in natural waters. Science 134, 98–99.

Ritchie, G.D., Shimmield, D.B., 1991. The use of ^{210}Po/^{210}Pb disequilibria in the study of the fate of marine particulate matter. In: Kershaw, P.J., Woodhead, D.S. (Eds.), Radionuclides in the study of marine processes. Elsevier, Amsterdam, pp. 142–153.

Rommets, J.W., Stoll, M.H.C., de Koster, R.X., de Bruin, T.F., de Baar, H.W., Bathmann, U.V., Smetacek, V., 1997. Database of the JGOFS expedition ANT X/6 aboard. R. V. Polarstern. Deep-Sea Research II 44 (1-2), 517–519.

Rutgers van der Loeff, M.M., Friedrich, J., Bathmann, U.V., 1997. Carbon export during the spring bloom at the Antarctic Polar Front, determined with the Natural Tracer ^{234}Th. Deep-Sea Research II 44, 457–478.

Rutgers van der Loeff, M.M., Buesseler, K., Bathmann, U.V., Hense, I., Andrews, J., 2001. Steady summer production and a sudden spring bloom make a comparable contribution to carbon and opal export near the Antarctic Polar Front, SE Atlantic. Deep-Sea Research II.

Sarin, M.M., Kim, G., Church, T.M., 1999. ^{210}Po and ^{210}Pb in the South-equatorial Atlantic: distribution and disequilibrium in the upper 500 m. Deep-Sea Research II 46, 907–917.

Shannon, L.V., Cherry, R.D., Orren, M.J., 1970. Polonium-210 and lead-210 in the marine environment. Geochimica et Cosmochimica Acta 34, 701–711.

Shimmield, G.B., Ritchie, G.D., Fileman, T.W., 1995. The impact of marginal ice zone processes on the distribution of

^{210}Po, ^{210}Pb and ^{234}Th and implications for new production in the Bellingshausen Sea, Antarctica. Deep-Sea Research II 42 (4–5), 1313–1335.

Smetacek, V., de Baar, H.J.W, Bathmann, U.V., Lochte, K., Rutgers van der Loeff, M.M., 1997. Ecology and biogeochemistry of the Antarctic Circumpolar Current during austral spring: a summary of Southern Ocean JGOFS cruise ANT-X/6 of R.V. Polarstern. Deep-Sea Research II 44, 1–22.

Turekian, K.K., Kharkhar, D.P., Thomson, J., 1974. The fates of ^{210}Pb and ^{210}Po in the ocean surface. Journal Rechargeable Atmosphere 8, 639–646.

Veth, C., Peeken, I., Scharek, R., 1997. Physical anatomy of fronts and surface waters in the acc near the 6°w meridian during austral spring 1992. Deep-Sea Research II 44, 23–49.

Wefer, G., Fischer, G., 1991. Annual primary production and export flux in the Southern Ocean from sediment trap data. Marine Chemistry 35, 597–614.

Whitworth III, T., Nowlin Jr., W.D., 1987. Water masses and currents of the Southern Ocean at the Greenwich Meridian. Journal of Geophysical Research 92 (C6), 6462–6476.